Journal of Material Science and Mechanical Engineering (JMSME)
p-ISSN: 2393-9095; e-ISSN: 2393-9109; Volume 4, Issue 3; April-June, 2017 pp. 118-125

http://www.krishisanskriti.org/Publication.html

Numerical Investigation of Heat Transfer Behaviour during Severe Accident in Indian PHWR

Mahesh Wakchaure[1], Sudhakar Umale[2] and Parimal Kulkarni[3]

[1]M.Tech Student, Sardar Patel College of Engineering, Mumbai-4000058
[2]Sardar Patel College of Engineering, Mumbai-4000058
[3]Scientific Officer (G) RED, Bhabha Atomic Research Centre, Mumbai-400085, India
E-mail: [1]wakchaurem258@gmail.com, [2]s_umale@spce.ac.in, [3]parimalk@barc.gov.in

Abstract—*In atomic energy plant, it is necessary to confirm safety against severe accident progression. The current study considers a numerical modelling of a hypothetic meltdown of fuel subassemblies as a result of low probability events with an intention to evaluate effects thermal load on calandria vessel. It is additionally meant to estimate the aptitude of calandria vessel in handling larger core meltdown accidents so as to demonstrate the capability of cooling core melt inside calandria vessel in Indian PHWR.*

CFD analysis has been performed on scaled test facility of an Indian Pressurized heavy water reactor with and without consideration of decay heat inside the corium melt. The temperature distributions inside the molten pool, across the vessel wall thickness and transient crust thickness variation were predicted employing the Ansys Fluent as a computational tool. The results demonstrated that presence of decay heat has serious effects on the coolability behaviour and development of crust within the molten pool. The simulated CFD results obtained are compared with the result obtained previously for with and without decay heat by experiment. Results show that the temperature profiles across vessel wall and in a molten pool are in great concurrence with experiment results.

1. INTRODUCTION

As post severe core damage accidents at Three Mile Island (1979), Chernobyl (1986) and Fukushima (2011) gave wake-up call to the nuclear industry and the regulatory authorities for prevention of a core-melt severe accident. Tokyo Electric report [1] emphasized that severe accidents had to be prevented and mitigated; and towards that purpose a knowledge-base on severe accidents had to be acquired.

India's current inland nuclear power program is based on the Pressurized Heavy Water Reactor (PHWR). The large cylindrical calandria vessel is consists several horizontal channels in Indian PHWR core. Each channel comprises a pressure tube and an external calandria tube. An insulating gas is filled between the calandria tube and pressure tube gap. Pressure tube contains the fuel with hot pressurized heavy water as a primary coolant. The fuel is natural UO_2 in the form of bundles of about 0.5 m lengths. The heavy water moderator is contained inside calandria vessel and each channel is submerged in it. The calandria vessel is surrounded by large vault water which removes decay heat from fuel. [2]. Fig.1 shows an illustrative view of PHWR core assembly.

A severe core damage accident has a very low probability due to incorporation of safety system in the design. However, in scenarios when an initiating event, like station blackout (SBO), loss of coolant accident (LOCA) [3] the fuel channels would heat up and fail. Due to this, core has become fully disassembled and corium bed is formed at the bottom of the calandria vessel. The melt transfers stored and decay heat to the calandria vault water. The integrity of calandria vessel depends on the thermal and structural loading.

Prasad et al. [4] performed the test to examine the melt coolability behaviour in a simulated PHWR calandria vessel using the calandria vault water by pouring simulant melt at 1200°C without decay heat. Another experiment by Prasad et al. [5] to quantify the effects of decay heat on the heat transfer behaviour and the thermal analysis on the calandria vessel wall. Decay heat in the melt pool was simulated using four high watt heaters cartridges, each having 3.2 kW. The transient temperature variations across the vessel wall thickness, inside the molten pool, and vault water were measured.

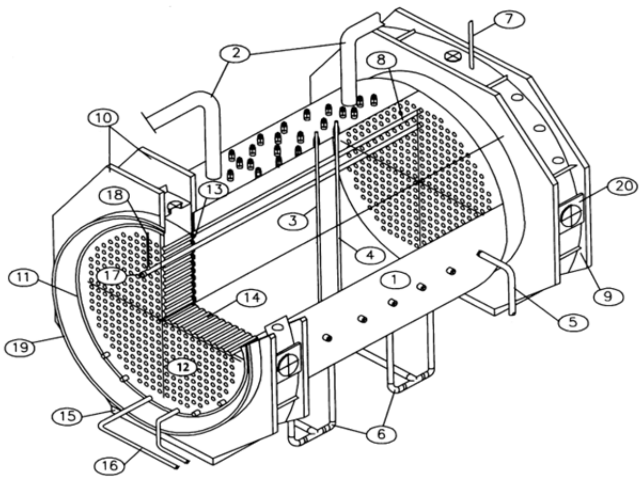

Fig. 1: PHWR core assembly [2].

1.Calandria Shell, 2.Over Pressure Relief Device, 3.Shut down System#1, 4.Shut Down System#1, 5.Moderator Inlet, 6.Moderator Outlet, 7.Vent Pipe, 8.Coolant Channel Assembly, 9.End Shield, 10.End Shield Support Structure Assembly, 11.Main Shell Assembly, 12.Tube Sheet, 13.Tube Sheet Cal Side, 14.Lattice Tube, 15.End Shield Support Plate, 16.End Shield Cooling Inlet Pipes, 17.End Fitting Assembly, 18.Feeder Pipe, 19.Outer Shell, 20.Support Lug.

Nicolici et al. [6] showed that comparison between CFD and PECM result in terms of maximum heat flux through calandria wall, maximum wall temperature and maximum melt pool temperature variations in time. The results estimated by the PECM approach are comparable within 10% with those obtained by the CFD method. Tran et al. Part-I [7] investigated correlation-based Effective Convectivity Model (ECM) for simulation of melt pool heat transfer in a light water reactor pressure vessel lower head. Tran et al. Part-II [8] estimated the assessments and representative application of the effective convectivity model (ECM) developed and described in the previous paper Tran et al. Part-I. Tran estimated that the ECM capability to accurately predict energy splitting and heat flux profiles in volumetrically heated liquid pools of different geometries over a range of conditions related to accident progression and validated against both experimental data and CFD results. Kudinov et al. [9] gave the approach of CFD method for molten corium coolability in a BWR lower head to confirm the physical soundness of the effective method simulation results.

David et al. [10] evaluated the heat removal capability of single tray core cacher design numerically and analyse the transient development of natural convection loops inside sodium cooled fast reactor pool. SFR pools are modeled with 1-D and 2-D axi-symmetric models and simulations demonstrated that the contribution of natural convection in the cooling of debris bed gets initiated within few minutes after debris settlement. Pavlidis et al. [11] provided an approach for multiphase flow modelling with phase change for numerical modelling of melt behaviour in the lower vessel head of nuclear reactor.

Review of the literature reveals that very few investigations are done on core melt behaviour in the lower plenum of the Indian PHWR. CFD simulation of test facility has been designed by Prasad et al. [4] need to be carried out. Consequently, it is logical to simultaneously pursue research on the existing PHWR designs for assessing their actual heat removal capabilities and innovative concepts for permitting the existing designs towards handling severe accidents.

In this regard, the current study has carried out natural convection fluid flow and heat transfer analysis on scaled test facility of Indian PHWR. In this, a considerable portion of simulant molten pool is settled on the lower head of calandria vessel of a test facility. Numerical analysis was carried out to validate CFD model with experimental data. The model was applied to estimate the heat transfer behaviour from the molten corium pool to the outside calandria vault water with and without considering of decay heat in the melt. The goal is likewise to pick up knowledge on the transient response of the reactor pool during Post Accident Heat Removal as a preliminary step towards building up the capability of vault water to evacuate decay heat for handling a severe accident in future Indian PHWR.

2. CFD SIMULATION OF MELT POOL FORMATION PHENOMENA

The present study is based on the following assumptions: 1) Pure conduction case: In this the case conduction debris bed is considered the only mode of heat removal from the debris bed. 2) The solid is homogeneously distributed in the mushy region. 3) The complex stratified temperature fields of the pools are not used in the present analysis. 4) The volume change upon phase change is ignored. 5) Sodium borosilicate glass in the liquid phase is considered an incompressible fluid.

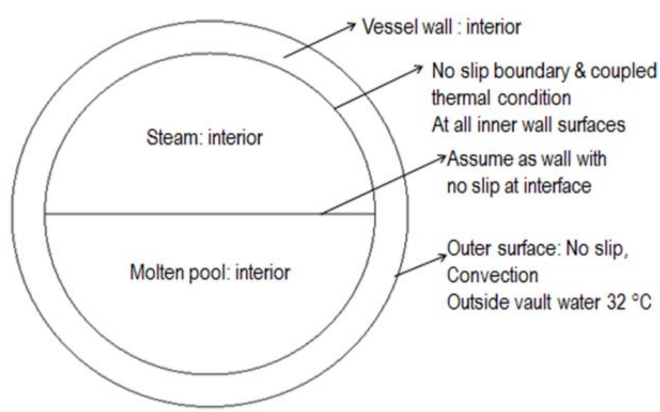

Fig. 2: 2-D model (no decay) with boundary conditions.

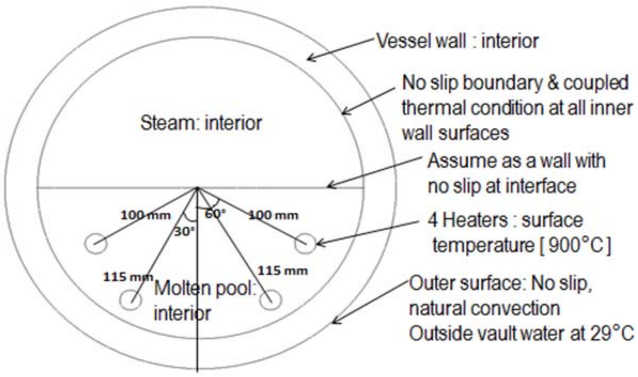

Fig. 3: 2-D model (with decay) with boundary conditions.

The upper surface of the molten pool/debris bed exchange heat with the vessel wall by thermal radiation and with the steam above the surface mainly by natural convection. The thermal conduction has been taken place through calandria wall to the shield tank water. The boundary conditions used for analysis of heat transfer from molten pool to outside vault water are shown in Fig. 2 and 3. For decay heat analysis, heater surface temperature is maintained at constant temperature 900°C with heat generation 0.7 MW/m^3 which are equivalents to the maximum power of 9.2 kW in the melt pool.

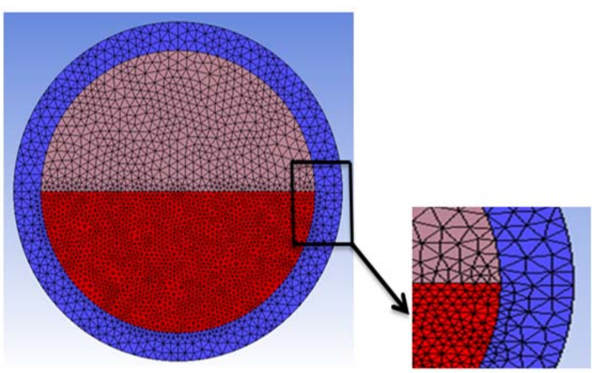

Fig. 4: Geometry meshing.

For the debris bed/melt pool, an unstructured grid was chosen with an element size of 4 mm. The vapour domain and calandria wall have meshed with unstructured grid elements with a maximum element size of 8 mm. In the present work, patch independent mesh method was used. An illustration of the domain mesh is presented in Fig.4.

The thermo-physical property for air is taken from the ANSYS FLUENT properties database. The characteristics of the calandria wall material and glass melt pool employed as follows: For calandria Wall (SS304L) properties are: Density: 7800 kg/m^3, Specific Heat: 500 J/kg.K, Thermal conductivity: 16 W/m.K and for molten material (Sodium Borosilicate glass) heat capacity calculated through: 200-1.5(T-1373) J/kg.K. The other properties are taken as constant: Density: 2200 kg/m^3, Thermal Conductivity: 1 W/m.K, Viscosity: 0.0025 Kg/m.sec, Solidus Temperature: 873 K, Liquidus Temperature: 1123 K, Pure solvent melting heat: 10^5 J / kg.

The emissivity of the calandria wall ε_{CS} is considered 0.3 and the emissivity of the upper surface of the debris bed ε_T is assumed to be 0.7 (for T > 1073 K) [12]. An UDF (User Defined Function) has been implemented to provide the local heat transfer coefficient values with a change in temperature with time. The Nusselt correlation for natural convection is estimated according to Churchill and Chu correlation [13].

$$Nu_{Avg}^{1/2} = 0.6 + 0.387\left\{\frac{Gr\,Pr}{[1+(\frac{0.559}{Pr})^{9/16}]^{16/9}}\right\}^{1/6} \quad (1)$$

For fully Developed nucleate boiling the heat transfer coefficient can be reproduced well by the simple empirical equation according to Fritz [14].

$$\alpha = 1.95\, q^{-0.72} p^{0.24} \quad (2)$$

The CFD calculations are carried out on the computational domain by solving the conservation equations for momentum and energy for transient natural convection with appropriate initial and boundary conditions using finite volume method.

For solidification/melting problems [15], the energy equation is:

$$\frac{\partial}{\partial t}(\rho H) + \Delta(\rho v H) = \Delta(k\,\Delta T) + S \quad (3)$$

Where, H = enthalpy; ρ = density; ν = fluid velocity and S = source term.

The enthalpy of the material is computed as:

$$\mathrm{H} = \mathrm{h_{ref}} + \int_{T_{ref}}^{\mathrm{T}} \mathrm{C_p}\, \mathrm{dT} + \frac{(\mathrm{T} - \mathrm{T_{solidus}})}{(\mathrm{T_{liquidus}} - \mathrm{T_{solidus}})} . \mathrm{L} \quad (4)$$

Where, h_{ref} = reference enthalpy; T_{ref} = reference temperature; C_p= specific heat at constant pressure and L= latent heat content.

The momentum sink due to the reduced porosity in the mushy zone is:

$$s = \left[\frac{(1+\beta)^2}{\beta^2+\epsilon}\right] A_{mush}\, ύ \quad (5)$$

Where, β is the liquid volume fraction; A_{mush} is the mushy zone constant; ϵ is a small number (0.001) to prevent division by zero and ύ is the solid velocity.

For the mushy zone constant the standard value of ANSYS FLUENT with C = 10^5 was used.

More importantly, there is a need to solve only the energy conservation equation without a need to follow instantaneous fluid motion. For the pressure-velocity coupling, the SIMPLE scheme, which is implemented in ANSYS FLUENT, was used for the present study. The PRESTO! spatial discretization algorithm is used for pressure with an under-relaxation factor of 1.0 for energy. Second order upwind scheme is used for the discretization of convection and diffusion terms in the conservation equations. Second order implicit formulation is used for the transient simulation. Convergence is assumed when the residual of energy is less than 10^{-6}.

At t = 0 sec, the temperature field for all domains is known: debris bed temperature 1100°C, vapour temperature 100°C and calandria wall temperature 32°C. The calandria vault water temperature is varied during the transient time is introduced using UDF.

3. RESULTS AND DISCUSSION

A grid independence test is carried out on geometry with different cell sizes 2946, 3937, 5802, 22099 and 86364 respectively. The element size of 5802 is selected for the investigation and numerical simulation, as the relative deviations of temperature are almost constant beyond this cell count irrespective of its cell size.

3.1 Analysis with no decay heat

The transient variation of temperature on vessel inner surface of the test section was predicted by using ANSYS CFD as shown in Fig.6 (a). By observing the temperature profile, it can be concluded that at location 0° (as shown in Fig.5) has higher temperature compared to location 45°, 90° and 180°. From this figure, it can be observed that at location 0°, 45° and 90° initially causes an increase in temperature of the inner surface and it tends to saturate after an hour. This is because, as soon as the melt is poured in the cylindrical test section, simulation results confirmed the formation of a thick crust. But at location 180°, the inner surface of the test section has the different trend of transient temperature profile was observed. This was due to the no crust formation and thermal resistance to heat transfer. It is seen from Fig.6 (b) that the same trend of transient temperature variation on the inner and outer surface of cylindrical test section was observed. Initially, the temperature of water rises very sharply followed by reduction before it reaches steady state. The initial peak in temperature was found more in a lower portion of test section compared to the upper portion of the test section.

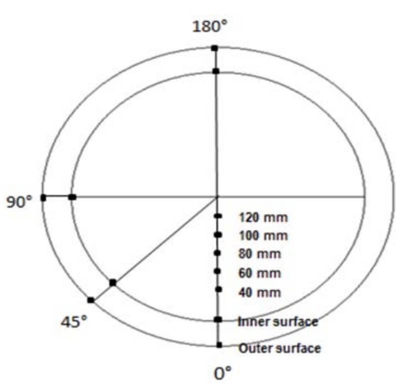

Fig. 5: Radial and Circumferential locations on test section.

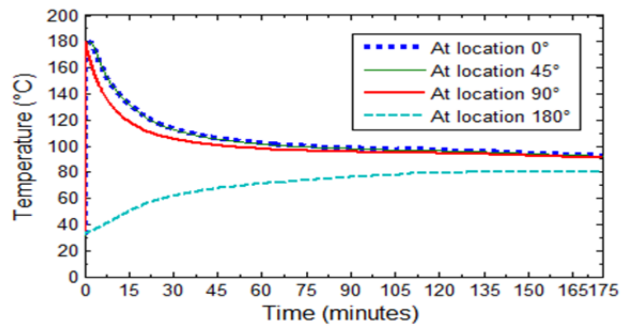

(a)

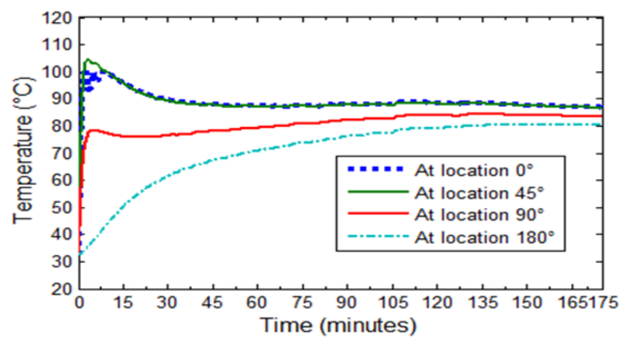

(b)

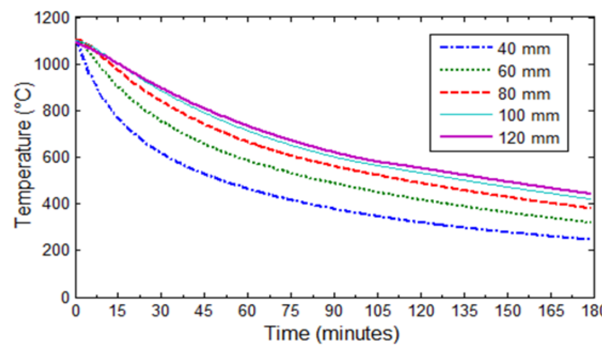

(c)

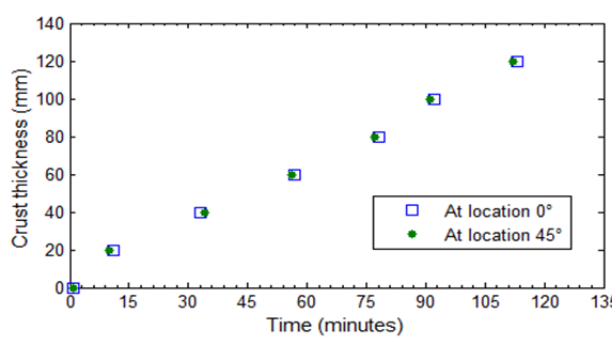

(d)

Fig. 6: Temperature distribution of test section at circumferential location 0°: (a) inner surface, (b) outer surface, (c) inside melt pool at location 0° at different radial locations, (d) Crust growth with time.

Fig.6(c) shows the temperatures inside the melt pool at 0° location (as shown in Fig.5) at different radial locations. It was observed that the rate of change of temperature reduces with radial height due to the formation of crust at bottom of the vessel which acts as an insulation, leading to high-temperature gradient inside molten pool along the radial direction. Fig.6 (d) shows the crust formation with time from the bottom of the cylindrical vessel. The crust growth thickness was changing almost linearly with time as there was no decay heat generation in the melt and heat transfer from the melt was mostly by conduction mode. The crust thickness variations at both 0° and 45° locations were identical since the temperature distributions were almost the same at both locations, and that is why the crust formation rate was almost the same.

3.2 Analysis with decay heat

Figs.7 (a) and 7 (b) show the CFD simulation results of temperature variation of inner and outer vessel surface at various circumferential locations. At the inner and outer surface, the maximum temperature of vessel surface was observed at 0° and 45°. It can be seen that at initial time step temperature of vessel inner and outer surface is rising suddenly to peak temperature then decreases. This was due to the formation of crust inside melt which offers resistance to heat transfer. Eventually, a steady state is reached, but after 50 min, the temperature of vessel inner and outer surface start was found to start increasing. This is due to the effect of decay heat generation inside the melt.

Fig.7 (c) shows the temperature variation of the heat generating melt pool at location 0° on different radial location. From the figure, it can be observed that initially the temperature of the melt was uniformly above 900°C and no temperature gradient was observed. However, with time non-uniform temperature gradient inside the melt pool along the radial direction was witnessed. Fig.7 (d) shows the crust formation with time from the bottom of the cylindrical vessel. Initially, the crust thickness grew linearly with time and after that, the crust thickness almost remained constant. The time required for constant crust thickness is different. This was due to the location of heaters at 45° near vessel wall as compared to location 0°.

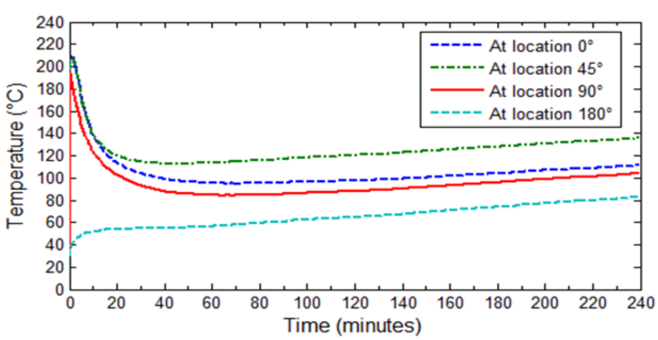

(a)

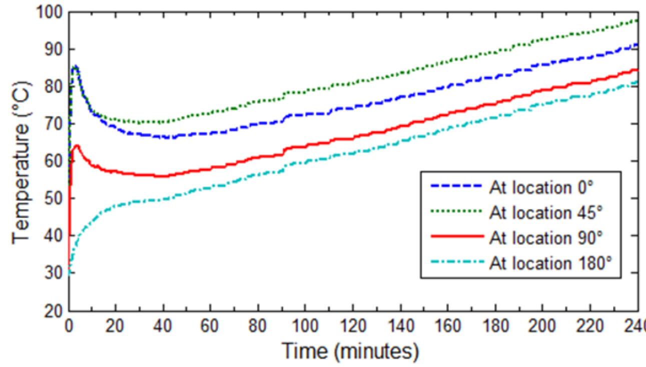

(b)

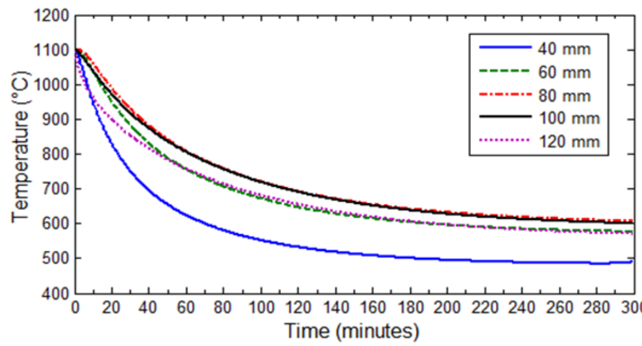

(c)

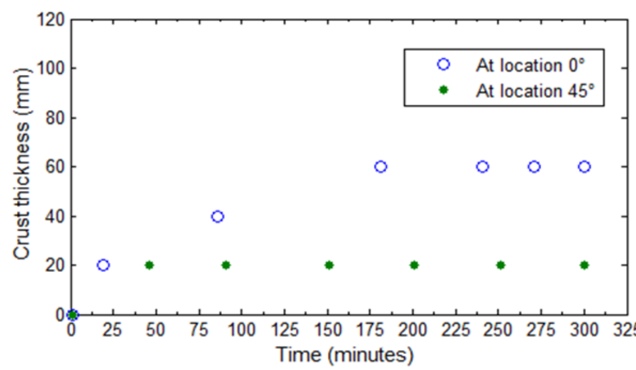

(d)

Fig. 7: Temperature distribution of test section at circumferential location 0°: (a) inner surface, (b) outer surface, (c) inside melt pool at location 0° at different radial locations and (d) Crust thickness variation with time.

3.3 Modal Validation

Model validation is an important step to ensure the correctness and reliability of the numerical model. In this present work, the results of the simulation are validated with the experimental test data.

A] Analysis with no decay heat

Fig.9 (a) shows the CFD simulation results of temperature variation on the inner surface and the outer surface (0°) as compared with experimental data. The deviation in temperatures of the vessel was due to geometry effect and assumption of the constant thermal conductivity of melt in the CFD model. At initial time 182°C was the peak temperature in the case of simulation and 196°C in the experimental results. The analysis shows that good agreement in temperatures on the inner and outer surface. In the case of CFD simulation at the initial time, free nucleate boiling of vault water occurs for short duration of time.

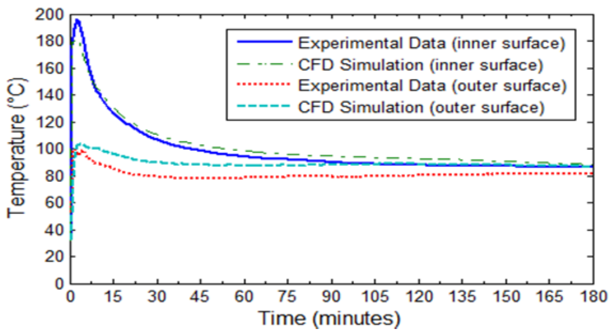

(a)

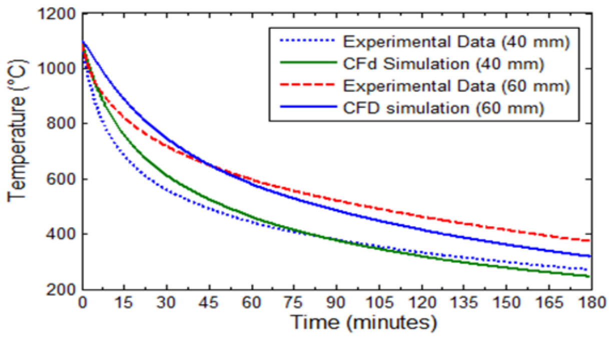

(b)

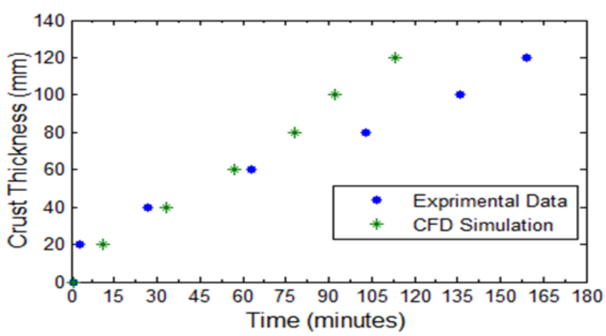

(c)

Fig. 9: Temperature distribution (no decay heat case) of test section on (a) inner and outer surface at 0° (b) inside molten pool at different radial heights 40 mm and 60 mm, and (c) Crust thickness variation with time.

Fig.9 (b) shows the transient temperature distribution in the molten pool inside test section at various radial heights from the bottom of test section 40 mm and 60 mm respectively. CFD simulation results were obtained to show the good agreement with the experimental data at various radial locations. From Fig.9 (c), it was observed that within two min (experimental) and eight min (CFD) from the pour of melt, the crust of nearly 20 mm thickness was formed and it took almost 158 min (experimental) and 112 min (CFD) to completely solidify the melt. In this analysis, uniform initial melt temperature was considered. However, at the start of experiments, initial high temperature gradient was observed inside melt. Due to this, significant differences between the crust thicknesses were observed.

B] Analysis with decay heat

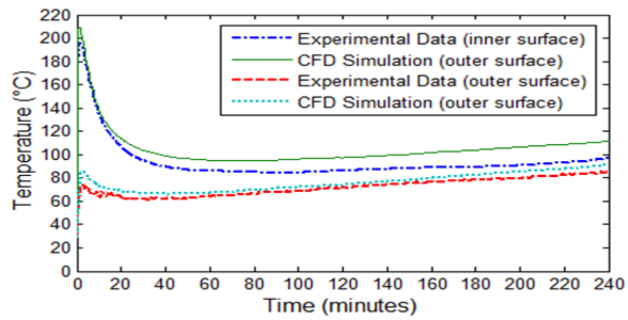

(a)

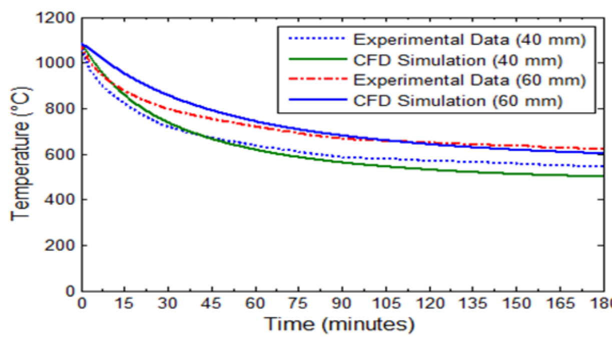

(b)

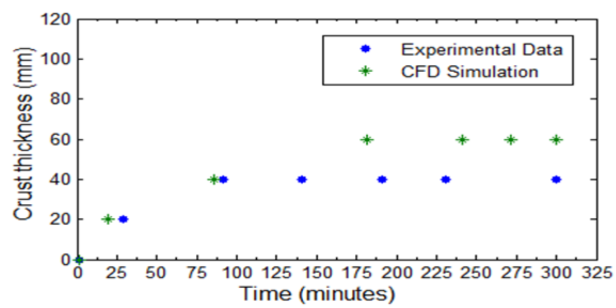

(c)

Fig. 10: Temperature distribution (decay heat case) of test section on (a) inner and outer surface at 0° (b) inside molten pool at different radial heights 40 mm and 60 mm, and (c) Crust thickness variation with time.

Fig.10 (a) shows the comparison of CFD model against experimental data on the inner and outer surface of calandria the vessel at circumferential location 0°. Peak Temperature on the inner surface of the vessel was found as 196°C (experimentally) and 209°C (CFD) respectively. On the other hand, Peak Temperature on the outer surface of the vessel was found as 75°C (experimentally) and 82°C (CFD) respectively. The variation in the vessel inner and outer surface temperatures 6.63 % and 9.33 % was observed.

Fig.10 (b) shows the transient temperature distribution with simulated decay heat generation in the molten pool inside test section at various radial heights from the bottom of test section 40 mm and 60 mm respectively. The effect of decay heat generation predicted earlier (~3.5 hr) in an experiment as compared CFD (~4.5 hr) from initial time step. Fig.10 (c) shows the crust thickness predicted by the CFD simulation and the experimental crust thickness. Crust thickness of CFD simulation is thicker compared with the experimental (60 mm vs 40 mm at radial location 0°). The larger CFD simulation crust thickness may be the effect of non-uniformly volumetric heating of the experiment (electrically heated heaters) compared with the uniformly volumetric heating of the CFD simulation that causes the cold liquid accumulated in the lowermost region to solidify.

3.4 Analysis of obtained results:

3.4.1 Determination of heat transfer and temperature across vessel wall

Instantaneous heat transfer across the cylindrical test section in the radial direction can be calculated [16] by using the heat transfer Eq. (6) and results are plotted in Fig.11.

$$Q = \frac{2\pi KL\Delta T}{\ln\left(\frac{r_o}{r_i}\right)} \quad (6)$$

Where, K - thermal conductivity of the vessel; Q-heat transfers rate; L- length of a cylinder; r_o- the outer radius of a cylinder; r_i- the inner radius of cylinder; ΔT- temperature difference across the vessel.

From Fig.11, it was observed that initially, there was a very high rate of heat transfer which drastically decreases with time and became almost constant. After an initial transient, the heat transfer was found to be uniform. In the case of decay heat (Simulation), maximum instantaneous heat transfer was found to be very high (~40 kW) which was approximately 62.5% more than the maximum instantaneous heat transfer (~32 kW) in case of no decay heat (Simulation). Fig.12 shows the variation of the temperature gradient (ΔT) across the cylindrical vessel thickness with time at location 0°. It was observed that initially, temperature difference across the vessel thickness was the highest (~157°C) with decay heat simulation. The variations of ΔT across the vessel thickness were found to decay with time and became more or less.

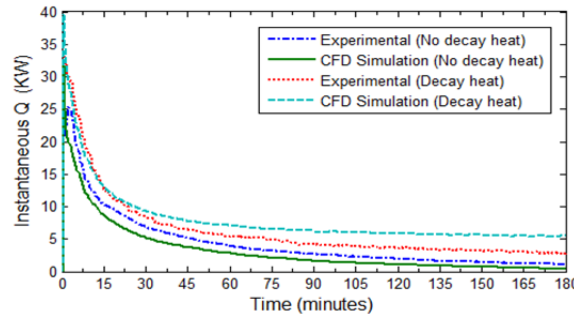

Fig. 11. Heat transfer rate variation with time.

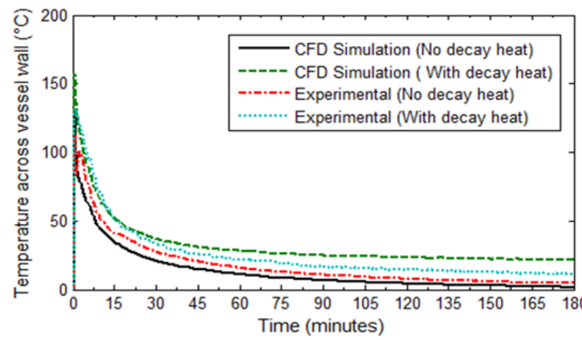

Fig. 12: Temperature across cylindrical vessel thickness with time.

3.4.2 Determination of local heat flux and heat transfer coefficient

The heat transfer coefficient and heat flux were calculated by using Eqs. (7) and (8) respectively [16].

$$KA\frac{dT}{dr} = hA(\Delta T) \quad (7)$$

$$\frac{Q}{A} = K\frac{dT}{dr} \quad (8)$$

Where, A- heat transfers area; h- local heat transfer coefficient; ΔT- temperature difference across the vessel; K- thermal conductivity; r- radius of a cylinder.

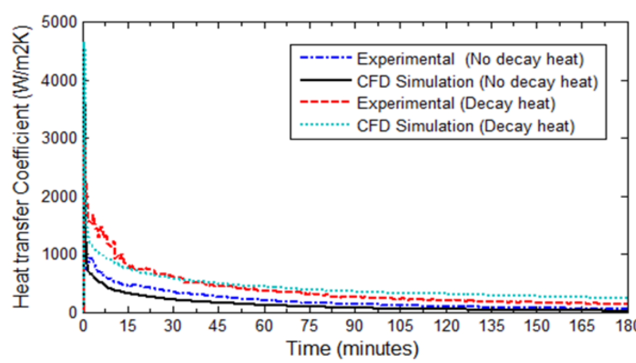

Fig. 13: Heat transfer coefficient variation.

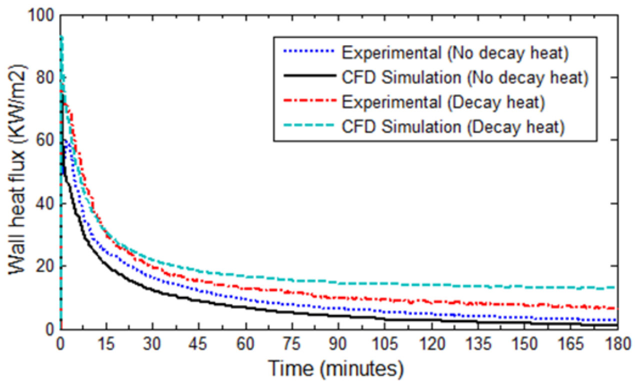

Fig. 14: Vessel wall heat flux variation with time.

Fig.13 shows the variation of heat transfer coefficient with time at location 0°. The heat transfer coefficient was found maximum at initial time step and then after suddenly drop below 1000 W/m^{2}k. The heat flux distribution on the wall follows the trend of ΔT variation across the wall as shown in Fig.14. On comparison of results, the value of temperature gradient across the cylindrical vessel thickness, the heat transfer coefficient and wall heat flux was found to be higher initially which decrease progressively with time in case of decay heat (Simulation).

4. CONCLUSION

The results of CFD simulations with ANSYS Fluent (14.0 version) package were validated against the available experimental data. The following inferences are drawn in the present study: As soon as the melt is poured in the cylindrical test section, CFD results confirmed the formation of a thick crust which introduced the high thermal resistance to heat transfer. It can be concluded that the melt initial temperature has little effect on heat transfer rate from the melt to the vault water. However, the coolability characteristics were not affected by no decay heat, but strongly affected by presence of decay heat. The maximum inner surface temperature of the vessel was 179°C and 209°C in no decay and with decay heat conditions respectively. The maximum outer surface temperature of the vessel was 100°C and 82°C in no decay and with decay heat conditions respectively. It was predicted that the integrity of vessel was intact for the given accident condition of the test facility. In the case of no decay heat, it was observed that crust thickness grew to substantial thickness, while in decay heat grew up slowly up to 60 mm and then it stabilized. In this study, the experimental results by Prasad et al.[4-5] has been shown to provide similar results within 15 % to those offered by the CFD model.

REFERENCES

[1] Fukushima Nuclear Accident Analysis Report, *Tokyo Electric Power Company, Inc,* 2012.

[2] Bajaj, S.S., Gore, A.R., "The Indian PHWR", *Nuclear Engineering and Design* 2006, 236 (7–8), 701–722.

[3] Kulkarni, P.P., Prasad, S.V., Nayak, A.K., Vijayan, P.K., "Thermal and structural analysis of calandria vessel of a PHWR during a severe accident", *Nuclear Engineering Technology* 2013, 45 (4), 463–476.

[4] Prasad, S.V., Nayak, A.K., Kulkarni, P.P., Vijayan, P.K., Vaze K.K., "Study on heat removal capability of calandria vault water from molten corium in calandria vessel during severe accident of a PHWR", *Nuclear Engineering and Design* 2015, 284, 130–142.

[5] Prasad, S.V., Nayak, A.K., "Experimental investigation of heat transfer during severe accident of a Pressurized Heavy Water Reactor with simulated decay heat generation in molten pool inside calandria vessel", *Nuclear Engineering and Design* 2016, 303, 75–87.

[6] Nicolici, S., Dupleac, D., Prisecaru, Ilie., "Numerical analysis of debris melting phenomena during late phase CANDU 6 severe accident" *Nuclear Engineering and Design* 2013, 254, 272–279.

[7] Tran, C.T., Dinh, T.N., "The effective convectivity model for simulation of melt pool heat transfer in a light water reactor pressure vessel lower head. Part I: physical processes, modeling and model implementation", *Progress in Nuclear Energy* 2009, 51 (8), 849–859.

[8] Tran, C.T., Dinh, T.N., "The effective convectivity model for simulation of melt pool heat transfer in a light water reactor pressure vessel lower head. Part II: model assessment and application", *Progress in Nuclear Energy* 2009, 51 (8), 860–871.

[9] Tran, C.T., Dinh, T.N., Kudinov, P., "An approach to numerical simulation and analysis of molten corium coolability in a boiling water reactor lower head", *Nuclear Engineering and Design* 2010, 240, 2148–2159.

[10] David, D.K., Mangarjuna Rao. P., Nashine, B.K., Selvaraj, p., Chellapandi, P., "Numerical simulation of passive heat removal under severe core meltdown scenario in a sodium cooled fast reactor", *Nuclear Engineering and Design* 2015, 291, 188-203.

[11] Pavlidisa, D., Gomesb, J. L. M. A., Xiec, Z., Paina, C. C., Tehranid, A. A. K., Moatamedie, M., Smitha, P. N., Jonesa, A. V., Matarc, O. K., "Numerical modelling of melt behaviour in the lower vessel head of a nuclear reactor", *Procedia IUTAM* 2015, 15, 72-77.

[12] Rogers, J.T., "Thermal and Hydraulic Behaviour of CANDU Cores under Severe Accident Conditions – Final Report Volume 1 – Analytical Methods and Results", *AECL, Ontario,* 1984.

[13] Welty, J.R., Wicks, C.E., Wilson, R.E., Rorrer, G.L., Fundamentals of Momentum Heat and Mass transfer, 5th ed. John Wiley and Sons, Hoboken, N.J, 2008.

[14] Baehr, H.D., Stephan, K., Fundamentals of Momentum, Heat and Mass transfer, 2nd ed. *Library of Congress*, Stuttgart, 2008.

[15] ANSYS Fluent 15 User's Guide Canonsburg PA 15317 ANSYS Inc. 243-45, 2014.

[16] Holman, J.P., Heat Transfer, 9th edition, *Tata McGraw Hill*, 2008.